

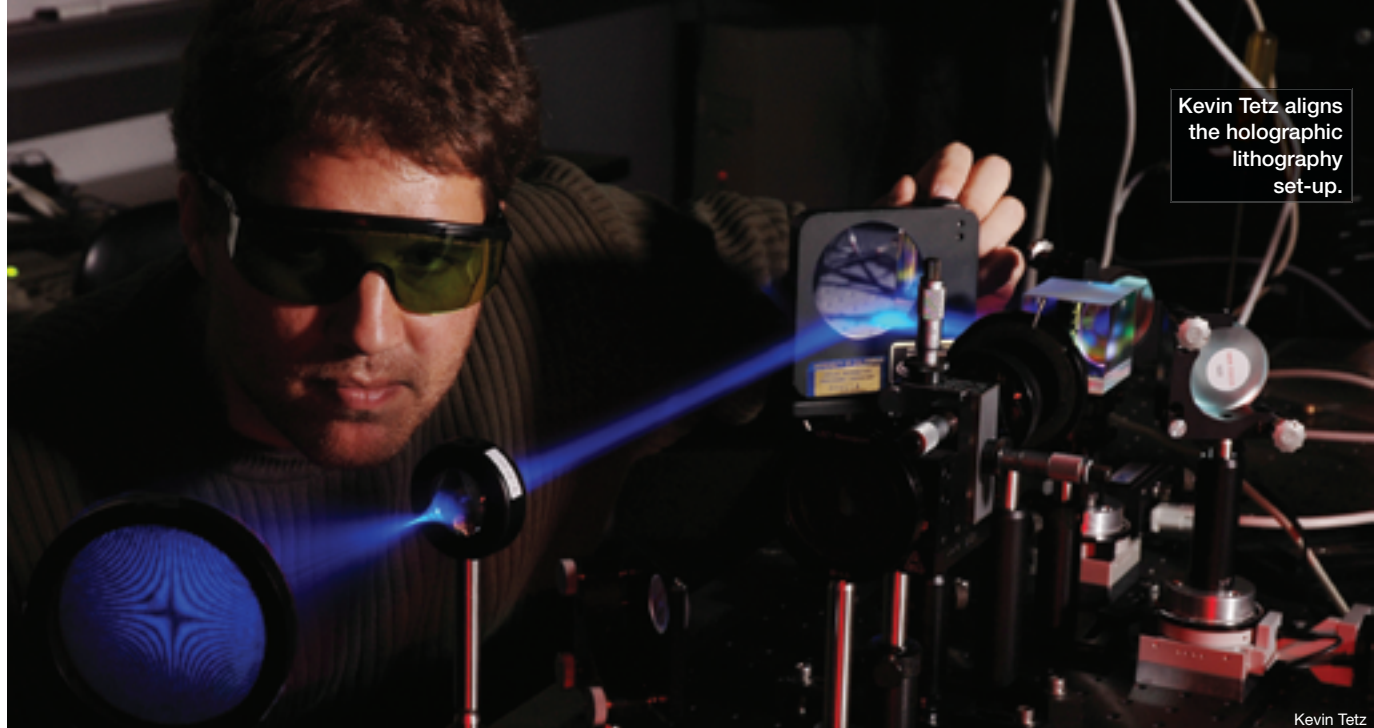
Kevin Tetz

The field of nanophotonics is finding myriad applications in information technology, health care, lighting, sensing and national security. This article explores the ultrafast electrodynamics of surface plasmon-polariton fields on nanostructured metal-dielectric boundaries, and describes how to make a sensor to measure chemical reactions at a surface by generating spatially resolved, reaction-dependent, spatial and spectral frequency information.

Surface Plasmonic Fields in

NANOPHOTONICS

Yeshaiahu Fainman, Kevin Tetz, Rostislav Rokitski and Lin Pang



Experts predict that nanolithography will reach a resolution of 16 nm by 2020, and that both top-down and bottom-up integration methods will become feasible, enabling reliable, scalable, power-efficient and cost-effective methods for the miniaturization of future systems. Over the past decade, significant progress has been made in the engineering of inhomogeneous composite materials (e.g., dielectrics, semiconductors, metals, organics, quantum dots) with unique optical properties such as polarization and spectral dispersion negative refraction, nonlinear polarization and quantum interference.

Recently, nanophotonic structures that involve optical modes at the interface between metallic and dielectric materials have attracted increasing attention. They exhibit intrinsic field localization at the interface between the media that facilitates nanoscale waveguiding and have the potential for full optical confinement to a nanoscale in three dimensions, reducing average power requirements for nonlinear wave mixing.

These unique features of surface plasmonic fields could lead to photonic devices that are much more compact than those achievable with current optical refraction technologies. Indeed, they may bridge the gap between photonics, biochemical sensing and CMOS-based electronics technologies.

Plasmons are the eigenmodes of collective density oscillations of quasi-free electrons (referring to the oscillations in metal materials). These oscillations occur at a characteristic frequency—the plasma frequency. In general, the plasma frequency and the resulting resonance oscillation characteristics are modified by the presence of an interface, and further affected if the metal has geometric structure on the length scale of the plasmon wavelength.

One common manifestation is in metallic resonant nanoparticles and spheroids, which have been studied extensively, most

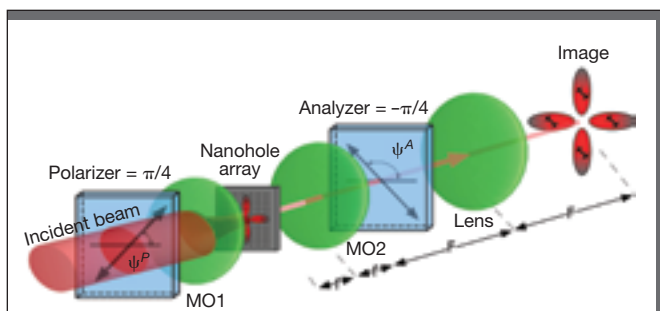
notably for their ability to enhance nonlinear wave mixing because of the plasmonic resonance field enhancements (huge field enhancements also occur in various places in the case of a “rough” metallic surface).

Surface plasmon polaritons

When a plasmon wave is coupled with a photon at an interface, it is described as a surface plasmon polariton (SPP). Due to this coupling between the photon and the electron gas, there is an effective binding energy (or momentum mismatch) that precludes coupling of a free space photon to the SPP in normal circumstances.

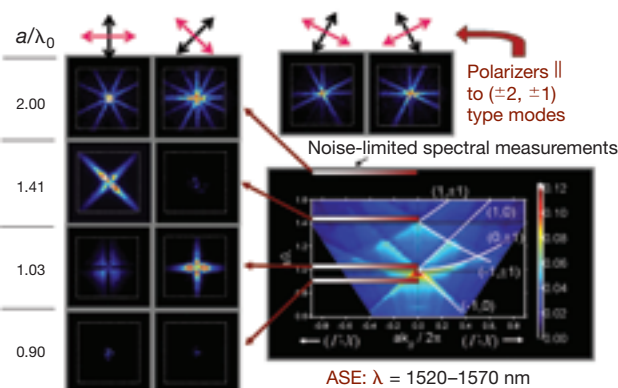
Typically, an incident photon needs some additional momentum to excite the SPP—most often acquired through evanescent coupling through a prism or via a grating. When the energy and momentum match precisely, there is a resonant excitation of the SPP. Indeed, researchers have shown that the plasma frequency and supported surface modes may be reduced to an arbitrarily low frequency by designing a proper surface structuring.

The scientific community’s interest in this area was recently sparked with the discovery of enhanced light transmission through nanoholes in an array or with surrounding surface corrugations. Even with a hole far below the cutoff of the enhanced fields, due to the resonant SPP excitation, the amount of light scattered through the holes was several times larger than expected for an isolated subwavelength hole. To achieve complete understanding of the in-plane SPP pulse, researchers must experimentally characterize SPP amplitude and phase evolution upon propagation, which presents an unexplored challenge—how to build practical nanophotonic devices for future information technologies.



Schematic diagram of SPP imaging configuration

A sample is illuminated using a focused laser (with a microscope objective). The resulting SPP mode is then imaged onto an InGaAs CCD array via a 4F imaging system (microscope objective and lens). The incident polarization at 45° is decomposed into two orthogonal components, which excite (1,0) type SPP modes that propagate along the grating surface and reradiate in forward and backward directions. The radiation is then polarized at -45° to obtain the field in the image plane.



Spectral measurements of unpolarized zero-order transmittance

Measurements for cubic arrays of holes in an aluminum film on a glass substrate. Data from arrays with different periods have been combined for these composite intensity images. The stitching frequencies appear as horizontal black lines [identical data are also replicated for $ak_{\parallel}/2\pi < 0$]. The SPP images were obtained using four samples with varying values of a/λ_0 . The polarizer-analyzer pair was arranged at 0°/90° for excitation and visualization of the $(\pm 1, \pm 1)$ type modes for nanohole array with $\lambda_0 = 1.41$ and at +45°/-45° for the $(\pm 1, 0)$ and $(0, \pm 1)$ type SPP modes for $a/\lambda_0 = 1.03$. Images of the higher order SPP modes obtained with laser illumination of nanohole arrays with $a/\lambda_0 = 2$. No SPP excitation is observed for the nanohole array with $a/\lambda_0 = 0.9$.

Ultrafast dynamics of SPP modes

In our experiments, we achieved excitation and visualization of ultrafast dynamics of SPP modes by coupling the optical field into and out of the metallic film using a 2D array of nanoholes etched in the metallic film on a dielectric substrate. We used several metals (Au, Ag and Al) with various substrate materials (glass, GaAs, Si) and adjusted the metal film thickness from 10 to 300 nm and the diameter of the nanoholes from 50 to 300 nm, with the array periods optimized for excitation of the desired SPP modes.

We characterized the samples optically using two illumination procedures: a collimated broadband light source for spectral measurements of the zero-order transmittance as a function of wavelength and incidence angle, and a focused laser beam of varying frequency to excite and image the propagating SPP scattered off the nanohole array.

For the spectral measurements, we collimated and polarized illumination from the lamp and imaged the central portion of the array onto the input slit of a monochromator, which scans a fixed spectral range of 1000 nm to 1700 nm. We used an InGaAs focal plane array for imaging and alignment. The figure on the left shows the measured zero-order unpolarized transmittance.

By measuring the transmittance for a number of samples with various periods, one can gain a better understanding of the modal structure of SPP fields. The spectra are dominated by asymmetric, Fano-type lineshapes at the various SPP excitation conditions. There are two components to this transmitted field: one that passes through the small, subwavelength holes directly, and one that is a product of the excited surface mode. The interference between these two components results in various maxima and minima.

The outlines of these major features of the dispersion map are described by the relation: $\vec{k}_{\text{SPP}} = \vec{k}_{\parallel} \pm i\vec{G}_x, \pm j\vec{G}_y$, where \vec{k}_{SPP} is the SPP wave vector, \vec{k}_{\parallel} is the in-plane component of the incident electromagnetic wave vector, and \vec{G}_x and \vec{G}_y are the reciprocal lattice vectors in the x and y directions, respectively. The dispersion curves we calculated for the air-metal (AM) interfaces [$+ak_{\parallel}/2\pi$ direction] follow well the SPP features for all of the data.

Excitation and propagation of the resonant modes

To understand the excitation and propagation process of the resonant modes, we constructed a laser-illuminated SPP imaging apparatus. We used a polarizer-analyzer pair to control the polarization state of the excitation field and the field in the

By measuring the transmittance for a number of samples with various periods, one can gain a better understanding of the modal structure of SPP fields.

image plane, and performed the excitation using a focused laser beam at normal incidence. In contrast to commonly used far-field measurements, this apparatus images the metal film with a nanohole array onto a CCD camera while simultaneously exciting with a range of incident wave vectors.

Scattering from SPPs observed under various conditions is shown on the left in the lower figure on the facing page, with each period-to-wavelength ratio labeled as an arrow at the corresponding frequency in the dispersion map on the right. At these positions, when the phase matching conditions are satisfied, an exponentially decaying SPP mode is excited in a direction dictated by the resultant vector. This is seen as crossed lobes extending out from the center of the illumination.

We obtained the SPP images using four samples with varying values of a/λ_0 . There was no SPP excitation for a nanohole array with a/λ_0 —which is the intersection of the angular intensity profile—and the period-to-wavelength ratio does not lead to excitation of any mode with appreciable efficiency. In all cases, the SPPs can only be observed to propagate to the end of the nanohole array, although they assuredly continue on the unmodulated surface.

Excitation and visualization of ultrafast electro-dynamics

We further extended our method to excite and visualize ultrafast electro-dynamics of the SPP fields using excitation with femtosecond laser pulses. For this investigation, we used a time-resolved version of the spatial heterodyne imaging technique, which provides the spatial distributions of the electromagnetic field amplitude and phase at different moments of time. We used a modified Mach-Zehnder interferometer to perform imaging of the SPP modes, and derived optical pulses with a central wavelength of 1550 nm and a temporal width FWHM of roughly 200 fs from a mode-locked laser. The pulses were then focused onto the center of the nanohole array through the substrate at the normal incidence with microscope objectives.

We performed time-resolved imaging using the spatial heterodyne technique. The reference optical pulse, derived from the same laser, is combined on the surface of the CCD with the image of the nanohole array scattering the femtosecond SPP pulse. The intensity profile of the resulting interference pattern was measured at various time delays between the reference laser pulse and the probe pulse incident upon the nanohole array. Each interference pattern is processed to obtain spatial distributions of the amplitude and phase for different delay values.

The inset in the top figure on the right shows the time-averaged SPP field, observed in the absence of the gating reference optical field. Four lobes of the observed field correspond to (1,0) and (0,1) SPP modes. Since the SPP is coupled out from the metal surface with appreciable efficiency only in the corrugation region, the SPP field is not visible outside of the nanohole array. In the presence of a short, time-gating optical pulse, the camera detects interference between the scattered femto-

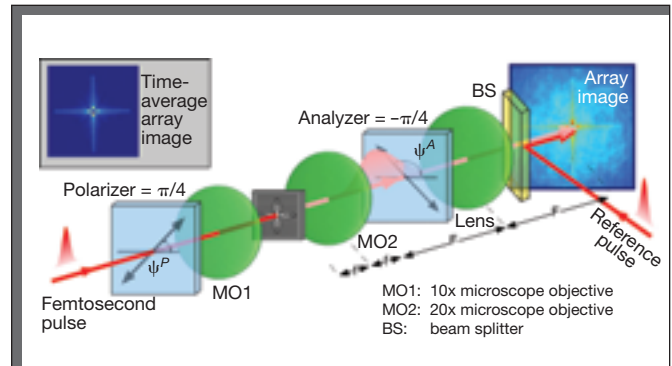
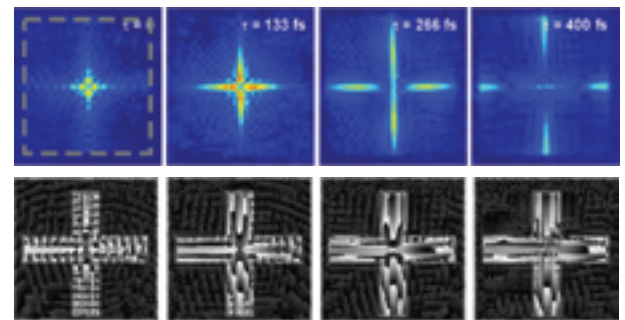


Diagram of excitation and time-resolved imaging of femtosecond SPP pulses

The nanohole array (200 x 200 μm size) is imaged with 40 times magnification on CCD surface, where the optical field, radiated by propagating SPP pulse forms interference with a superimposed femtosecond reference pulse. The interference pattern is shown in false color for $\Delta\tau = 0.5$ ps delay between pulses. A crossed polarizer/analyzer pair blocks the transmitted optical field while passing the scattered SPP field. The inset SPP field was detected without a reference femtosecond pulse.



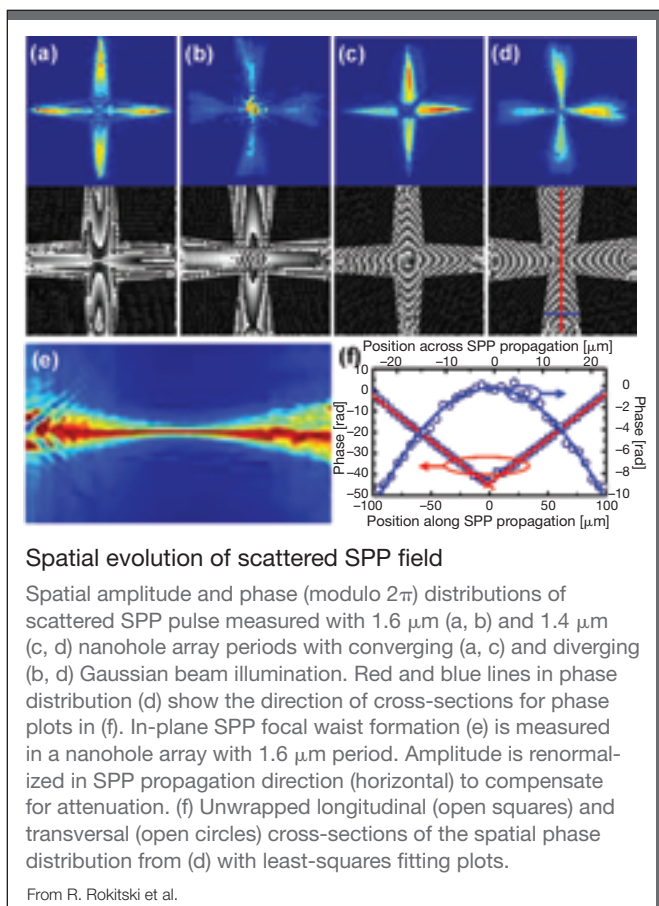
Temporal evolution of scattered femtosecond SPP pulse images

Spatial amplitude (top row) and phase (bottom row) of the femtosecond SPP pulse (shown in false color) scattered from a nanohole array with 1.6 μm hole period, measured for several time delays between SPP and reference pulses. Dashed line outlines the dimensions of the nanohole array.

From R. Rokitski et al.

second SPP pulse and the reference pulse when they overlap in time and space. The light intensity field recorded by the camera corresponds to optical field cross-correlation of the waveforms of the SPP and the reference pulse at a given time delay.

The figure (above, lower) shows images that represent spatial amplitude and phase distributions at four different delays between the interfering fields: $\Delta\tau = 0, 133, 266$ and 400 fs for the nanohole array, with $a = 1.6 \mu\text{m}$. The weakly focused incident optical wave satisfies the phase-matching condition for launching four SPP modes diverging along the array axes [i.e., (1,0) and (0,1)]. The amplitude distributions at short time delays reveal significant spatial modulation of the amplitude of the field, which is absent at longer time delays. We attribute



this amplitude modulation to spatial interference between four femtosecond SPP pulses propagating toward the center of the SPP excitation region.

At the short time delays, the four excited SPP pulses overlap in the center of the array forming the SPP modal interference pattern. At longer delays the pulses pass through the center, separate spatially, and no interference is observed.

Spatial distributions of SPP waves

We also investigated the relation between the optical phase and the phase of the excited SPP fields by modulating the spatial phase of the ultrashort excitation pulse. The spatial phase map of the propagating femtosecond SPP field was recorded in two nanohole arrays with periods $a = 1.4$ and $1.6\ \mu\text{m}$, supporting $(-1,0)$, $(0,-1)$ and $(1,0)$, $(0,1)$ SPP modes. The nanohole arrays were illuminated with converging and diverging Gaussian beams.

The figure below includes snapshots of spatial distributions of amplitude and phase of the SPP waves recorded at fixed delays between the probe and reference femtosecond pulses. The spatial amplitude distributions demonstrate that, when the nanohole arrays are illuminated with a converging Gaussian beam, the excited SPP wave also converges and focuses. Conversely, when the arrays are illuminated with diverging Gaussian beams, the SPP waves diverge from the illumination point and their amplitudes decay accordingly.

When the converging SPP wave is excited on an edge of the array, its propagation can be observed over a distance of $200\ \mu\text{m}$, and one can clearly see focusing of the SPP wave to a small transverse dimension and its divergence past the focal point. While the surface field reaches maximum spatial localization (i.e., minimal transverse field profile) at the focal point, the absolute wave power is reduced due to the damping.

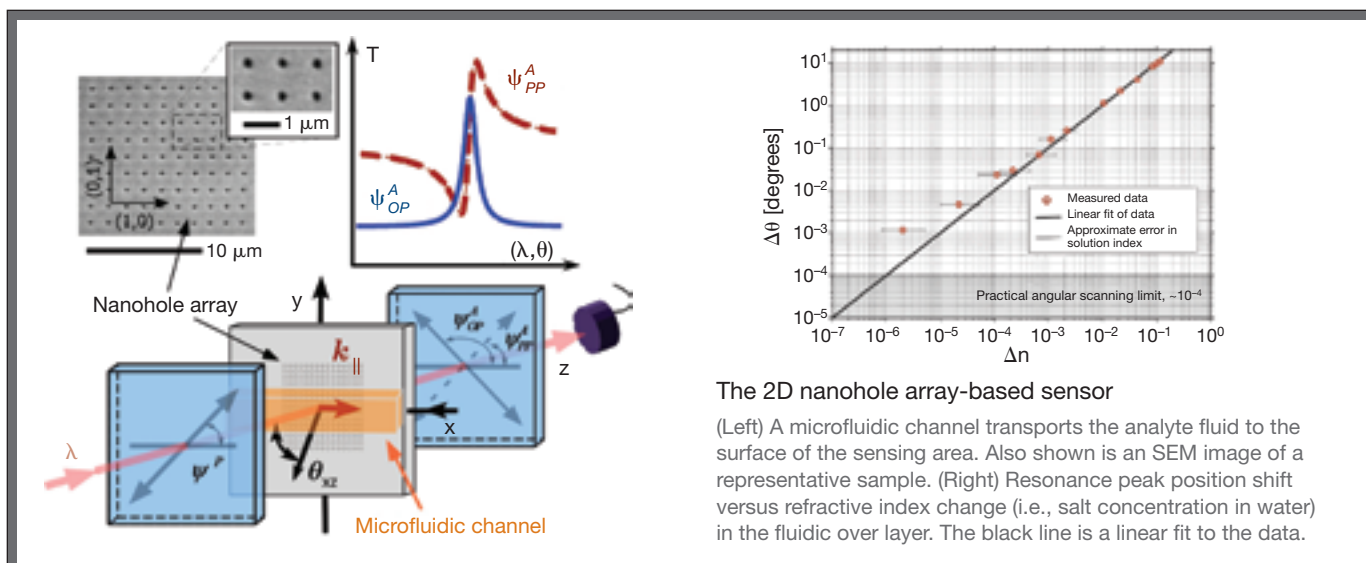
Spatial distributions of the SPP phase show several characteristic features of the scattered SPP fields. A cross-section of the spatial phase profile along the SPP propagation indicates linear phase variation. The amount of this linear phase corresponds directly to the angle of incidence of the free space optical wave, which is coupled to the SPP most efficiently. As we expected, the magnitude of the linear phase is the same for converging and diverging beam illumination. Transverse phase distributions for both arrays have close to quadratic profiles, implying converging and diverging propagation of the surface field.

Achieving excitation of femtosecond SPP pulses and observing them using the time-resolved spatial heterodyne imaging are important steps toward understanding the connection between spatial and temporal characteristics of the incident optical waves and of the excited and scattered SPP waves. The focusing of the femtosecond SPP pulses leads to complete localization of the electromagnetic field in space and time—which is essential for various applications in sensing, nonlinear optics and biomedical imaging.

Surface plasmon resonance (SPR) sensors

The results of our recent studies on excitation, propagation and scattering of the SPP fields in 2D nanohole arrays illuminate how to develop a high spectral resolution surface plasmon resonance (SPR) sensor that operates at normal or near normal incidence, facilitating high spatial resolution imaging. The samples for our SPP sensor experiments are fabricated by depositing gold films on a glass substrate followed by holographic lithography to achieve large usable areas (about $1\ \text{cm}^2$).

The focusing of the femtosecond SPP pulses leads to complete localization of the electromagnetic field in space and time—which is essential for various applications in sensing, nonlinear optics and biomedical imaging.



The 2D nanohole array-based sensor

(Left) A microfluidic channel transports the analyte fluid to the surface of the sensing area. Also shown is an SEM image of a representative sample. (Right) Resonance peak position shift versus refractive index change (i.e., salt concentration in water) in the fluidic over layer. The black line is a linear fit to the data.

Multiple exposures of SU-8 resist yield a 2D array of nanoholes with fine control of about 200 nm in hole diameter. We then transfer the holes into gold film using ICP/RIE dry etching and bond a polydimethylsiloxane (PDMS) mold with microfluidic delivery channel 1 cm \times 2 mm \times 100 μm to the substrate by oxygen plasma. The measurements are carried out using a setup shown schematically in the figure above, similar to the experiments on imaging SPP using a crossed polarizer-analyzer pair, though the illumination is with a plane wave.

When the polarizer-analyzer pair is parallel, we get Fano-type transmission lines. However, when the polarizers are orthogonal, the background radiation is suppressed, and there is only a pure resonance (Lorentzian) transmission line. The surface wave is excited by a projection of the incident electric field polarization in the propagation direction, and the reradiated field is again projected onto the analyzer. This linewidth is narrower in both frequency and angular width (maximizing resolution), and thus can be used to monitor changes effectively in the local refractive index of the surface. Schematics of the normalized transmittance spectra for both wavelength and angular interrogation are shown in the vicinity of $[-1, 0]$ type SPP modes.

For sensor characterization, we performed resonant transmission experiments using angular and wavelength interrogation exciting $[+1, 0]$ type SPP modes and varied the refractive index of the overlayer fluid (varying concentrations of Na_2CrO_4 in H_2O). As the SPP mode was maximal at the interface between the metal and dielectric layer, the sensor was extremely sensitive to perturbations at this surface, and could be used to monitor chemical reactions of various types by attaching molecules to the surface and supplying appropriate probe molecules of interest in the analyte fluid.

We have optimized the angular and spectral transmittance of the structure to a pure Lorentzian lineshape, leading to a linewidth narrowing that maximizes the sensor resolution,

which we show to be of $O(10^{-5})$ RIU. We estimate the potential of this system of $O(10^{-6})$ RIU under optimal conditions, with a nonabsorbing overlayer.

In the future, the ultrafast SPP combined with optofluidics will have a significant impact on various applications, including nanometrology, nanoscale spectroscopy, live cell dynamics, sensing, hyper-spectral imaging of biological species and nanotomography. Investigation of opto-plasmonic fields and their control on a nanoscale has the potential to lead to new tools to further advance cell biology and medicine. Δ

The authors acknowledge the support of NSF, The DARPA Center for Optofluidics and AFOSR.

Yeshaiahu (Shaya) Fainman (fainman@ece.ucsd.edu), Kevin Tetz (ktetz@ece.ucsd.edu) and Lin Pang (lpang@ece.ucsd.edu) are with the department of electrical and computer engineering at the University of California, San Diego, and Rostislav Rokitski is with Cymer Corp., Rancho Bernardo, Calif.



[References and Resources]

- >> M. van Exter and A. Lagendijk. Phys. Rev. Lett. **60**, 1 (1988).
- >> H. Raether. *Surface Plasmons on Smooth and Rough Surfaces and on Gratings*. Springer-Verlag, 1988.
- >> T.W. Ebbesen et al. Nature **391**, 667 (1998).
- >> A. Dogariu et al. Opt. Lett. **26**, 7 (2001).
- >> L. Martin-Moreno et al. Phys. Rev. Lett. **86**, 1114 (2001).
- >> Y.-H. Liao et al. Opt. Lett. **27**, 10 (2002).
- >> E. Altewischer et al. JOSA B, **20**, 9 (2003).
- >> W.L. Barnes et al. Nature **424**, 824 (2003).
- >> J. Homola. "Present and future of surface plasmon resonance biosensors," Anal. Bioanal. Chem. **377**(3), 528-39 (2003).
- >> W.L. Barnes et al. Phys. Rev. B **92**, 107401 (2004).
- >> S.M. Williams et al. Nanotechnology **15**(10), S495-S503 (2004).
- >> Y. Alaverdyan et al. Nano Lett. **5**(11), 2335-9 (2005).
- >> R. Rokitski et al. Phys. Rev. Lett. **95**(17), 177401/1-4 (Oct. 2005).
- >> K. Tetz et al. Appl. Phys. Lett. **86**, 111110 (2005).
- >> K. Tetz et al. Opt. Lett. **31**(10), 1528-30 (May 2006)